Unveiling the Non-Abelian Statistics of $D(S_3)$ Anyons Using a Classical Photonic Simulator

Unveiling the Non-Abelian Statistics of $D(S_3)$ Anyons Using a Classical Photonic Simulator

Suraj Goel,[1,*] Matthew Reynolds,[2,*] Matthew Girling,[2] Will McCutcheon,[1] Saroch Leedumrongwatthanakun,[1] Vatshal Srivastav,[1] David Jennings,[2,3] Mehul Malik,[1,†] and Jiannis K. Pachos[4,‡]

[1]*Institute of Photonics and Quantum Sciences, Heriot-Watt University, Edinburgh EH14 4AS, United Kingdom*
[2]*School of Physics and Astronomy, University of Leeds, Leeds LS2 9JT, United Kingdom*
[3]*Department of Physics, Imperial College London, London SW7 2AZ, United Kingdom*
[4]*School of Physics and Astronomy, University of Leeds, Leeds LS2 9JT, United Kingdom*

(Received 20 April 2023; revised 16 January 2024; accepted 22 February 2024; published 13 March 2024)

Simulators can realize novel phenomena by separating them from the complexities of a full physical implementation. Here, we put forward a scheme that can simulate the exotic statistics of $D(S_3)$ non-Abelian anyons with minimal resources. The qudit lattice representation of this planar code supports local encoding of $D(S_3)$ anyons. As a proof-of-principle demonstration, we employ a classical photonic simulator to encode a single qutrit and manipulate it to perform the fusion and braiding properties of non-Abelian $D(S_3)$ anyons. The photonic technology allows us to perform the required nonunitary operations with much higher fidelity than what can be achieved with current quantum computers. Our approach can be directly generalized to larger systems or to different anyonic models, thus enabling advances in the exploration of quantum error correction and fundamental physics alike.

DOI: 10.1103/PhysRevLett.132.110601

Introduction.—The exotic statistics of non-Abelian anyons make them of interest in fundamental physics [1–5]. In addition, their resilience to local perturbations has given rise to several schemes for topological quantum computing and other applications [6–10]. This behavior is key for fault-tolerant quantum computing, making non-Abelian anyons a potential solution to error problems that limit the scaling of quantum computers [10–12]. In the last decade we witnessed an intense effort to identify signatures of non-Abelian anyons in various physical platforms, such as fractional quantum Hall liquids at $\nu = 5/2$ [13], $p + ip$ topological superconductors [14,15], or quantum wires [8]. Unfortunately, the complexity of these systems allows for an alternative interpretation of the observed signatures [16]. The conclusive characteristic of non-Abelian anyons is their exchange statistics, which are currently too complex to realize in the laboratory.

At the same time, several investigations have focused on simulating non-Abelian anyons [17–22]. These efforts aim to establish the necessary conditions for observing non-Abelian statistics and addressing technical challenges in scaling and accuracy. Often, such simulations suffer from key loopholes. For example, the simulation of Majorana fermions utilizes a nonlocal encoding of fermionlike anyonic states in many qubits, with the help of the Jordan-Wigner transformation. However, this nonlocal encoding lacks the desired topological stability against local errors inherent in anyonic systems.

Here, we propose a photonic simulation of non-Abelian anyon statistics corresponding to the $D(S_3)$ planar code [11] and implement classical photonic manipulations to demonstrate its core features. Planar codes are both quantum error-correcting codes and condensed matter systems that host anyonic excitations. Although they require many-body interactions, their local encoding on spins makes them attractive for quantum simulations. The simplest version of the planar code is the toric code that supports Abelian anyons. The toric code has been already simulated in the laboratory with Josephson junctions [23] and photonic systems [24,25].

We introduce a novel method to minimally encode the core manipulations of $D(S_3)$ non-Abelian anyons, which enables us to demonstrate that a single qutrit is sufficient to reveal their non-Abelian fusion and braiding properties. The operations required to generate and manipulate anyons are in general nonunitary matrices that have a unitary action on the anyonic Hilbert space [26–28]. The implementation of nonunitary operations is typically experimentally challenging with current quantum computing architecture. To overcome this problem we develop a novel photonic technique that allows us to accurately perform these nonunitary operations with high fidelity, thus enabling us to demonstrate non-Abelian statistics using a classical

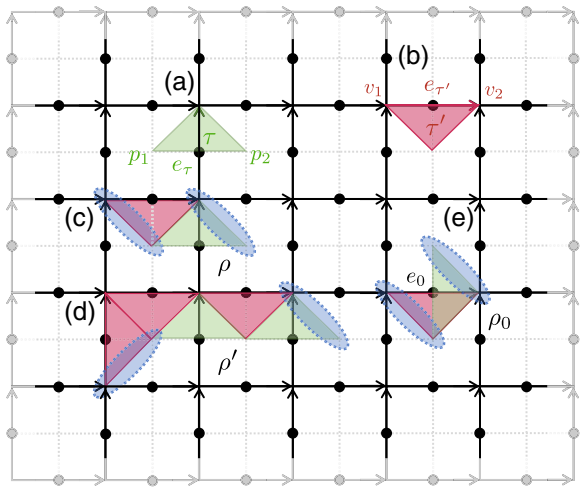

FIG. 1. Ribbon operators of G anyons. (a) A dual triangle τ has support on link e_τ and creates excitations at p_1 and p_2 plaquettes. (b) A direct operator τ' has support on link $e_{\tau'}$ and create excitations at v_1 and v_2 vertices. (c),(d) Compositions of dual and direct triangles give rise to ribbon operators ρ. Anyonic excitations of ribbon operators are dyons (dotted ovals) that are positioned at the endpoint plaquettes and vertices. (e) We define the elementary ribbon ρ_0 where both dual and direct triangles have support on the *same* link e_0.

photonic simulation. This minimal anyonic simulation will inform future pursuits that aim to probe more complex physics, such as topological error correction and avoidance, by optimizing the required resources and providing practical methods to realize their evolution. Our Letter can be expanded in two directions with advancements in technology. First, it can be scaled to larger lattice systems, allowing for a broader range of anyonic operations. Second, Hamiltonian interactions can be added to provide active fault tolerance in the topologically encoded quantum information.

The non-Abelian $D(S_3)$ anyonic model.—The $D(S_3)$ model is based on the group transformations of a triangle, $S_3 = \{e, c, c^2, t, tc, tc^2\}$, where e is the identity element, c the generator of $2\pi/3$ rotations, and t the generator of reflections. The $D(S_3)$ planar code consists of a square lattice where $d = 6$ qudits are positioned at its links parametrized by the group elements of S_3, as shown in Fig. 1. The Hamiltonian of the model has mutually commuting plaquette and vertex operators [11]. The ground state of the model is identified as the vacuum and its anyons are manifested as localized excitations at the vertices and/or the plaquettes.

This $D(S_3)$ planar code supports eight different anyonic excitations labeled by $\{A, B, C, D, E, F, G, H\}$ [29–31]. Particle A corresponds to the vacuum that fuses trivially with the rest of the anyons. Here, we restrict ourselves to the $\{A, B, G\}$ subgroup that is closed under fusion, $B \times B = A$, $G \times B = G$, and $G \times G = A + B + G$. Moreover, G has nontrivial braiding statistics. Its corresponding fusion, F^G_{GGG}, and braiding, R^{GG}, unitary matrices are given by

$$F^G_{GGG} = \frac{1}{2}\begin{pmatrix} 1 & 1 & \sqrt{2} \\ 1 & 1 & -\sqrt{2} \\ \sqrt{2} & -\sqrt{2} & 0 \end{pmatrix}, \quad R^{GG} = \begin{pmatrix} \bar{\omega} & 0 & 0 \\ 0 & \bar{\omega} & 0 \\ 0 & 0 & \omega \end{pmatrix}, \quad (1)$$

where $\omega = e^{2\pi i/3}$, which give a nontrivial braiding matrix $B^{GG} = FR^2F^\dagger$. The non-Abelian character of the G anyons is manifested in the nontrivial commutation relation between F^G_{GGG} and $(R^{GG})^2$. The $\{A, B, G\}$ subgroup should be contrasted to $\{A, B, C\}$, which has similar fusion rules but trivial braiding statistics, $B^{CC} = \mathbb{1}$ [30,32].

It is possible to verify fusion and braiding properties of the planar code anyons by generating and manipulating the corresponding anyonic excitations. Such excitations are created from the vacuum state by applying operations on the links of the lattice. In general, these rotations are given in terms of ribbon operators F^X_ρ, where ρ is the path along which the rotations are applied, giving rise to two X anyons at its endpoints. These ribbon operators, together with their action on the ground state, encode the anyonic fusion and braiding properties.

To define the ribbon operators we employ the oriented lattice representation of $D(S_3)$ shown in Fig. 1. A dual triangle τ has support on a link e_τ and is connecting two plaquettes p_1 and p_2 adjacent to the link e_τ, as shown in Fig. 1(a). A direct triangle τ' has support on a link $e_{\tau'}$ and is connecting two vertices v_1 and v_2 adjacent to the link $e_{\tau'}$, as shown in Fig. 1(b). We now assign a six-dimensional Hilbert space, $\{|h\rangle, h \in S_3\}$, to each link e_τ. To every triangle τ we define an operator $L^h_{\tau_{\text{dual}}} = \sum_{g\in S_3} |hg\rangle\langle g|$, with $h \in S_3$, acting on e_τ, if e_τ points toward v. Otherwise $L^h_{\tau_{\text{dual}}} = \sum_{g\in S_3} |gh^{-1}\rangle\langle g|$. Similarly, we define $P^g_{\tau_{\text{dir}}} = |g\rangle\langle g|$, with $g \in S_3$, if e_τ is clockwise with respect to p, otherwise $P^g_{\tau_{\text{dir}}} = |g^{-1}\rangle\langle g^{-1}|$. We next define the composite operators $F^{h,g}_\rho = L^h_{\tau_{\text{dual}}} P^g_{\tau_{\text{dir}}}$, where $\rho = \tau_{\text{dir}}\tau_{\text{dual}}$ with τ_{dir} a direct and τ_{dual} a dual triangle. Ribbon operators, F^X_ρ, that give rise to X anyons are built out of such matrix elements, $F^{h,g}_\rho$, acting on qudits [30].

The A and B anyons are constructed from strings of operators corresponding to direct τ's. They give rise to anyons positioned at vertices, i.e., they have $h = e$ with $L^e = \mathbb{1}$. Similar to the toric code's e and m anyons the A and B anyons can be created and moved around by applying single qudit unitary operator, F^A_τ and F^B_τ, to a string of qudits [11], where

$$F^A_\tau = |e\rangle\langle e| + |c\rangle\langle c| + |c^2\rangle\langle c^2| + |t\rangle\langle t| + |tc\rangle\langle tc| + |tc^2\rangle\langle tc^2|,$$
$$F^B_\tau = |e\rangle\langle e| + |c\rangle\langle c| + |c^2\rangle\langle c^2| - |t\rangle\langle t| - |tc\rangle\langle tc| - |tc^2\rangle\langle tc^2|. \quad (2)$$

Note that F^A is the identity operator acting on the qudit and both F^A and F^B are unitary matrices whose sum, $F^A_\tau + F^B_\tau = 2(|e\rangle\langle e| + |c\rangle\langle c| + |c^2\rangle\langle c^2|)$, can be described by a single qutrit operator.

The G non-Abelian anyons are dyonic, i.e., it includes both direct and dual triangle operators forming ribbons. Dyons are positioned at composite plaquette and vertex at each of the endpoints of the ribbon, as shown in Figs. 1(c)–1(e). A simple way to create a pair of G anyons on neighboring vertices and plaquettes is to use the ribbon $\rho = \tau_{\text{dual}}\tau_{\text{dir}}$ [31], as shown in Fig. 1(c). The corresponding ribbon operator is given by

$$F^G_\rho = F^{c,e}_\rho + \omega F^{c,c}_\rho + \bar{\omega} F^{c,c^2}_\rho + F^{c^2,e}_\rho + \bar{\omega} F^{c^2,c}_\rho + \omega F^{c^2,c^2}_\rho, \quad (3)$$

where for simplicity we omitted the overall normalization. One can show that F^G_ρ is Hermitian but not unitary. Nevertheless, its restriction to the eigenstates of the $D(S_3)$ Hamiltonian are unitary [26]. Finally, note that larger ribbon operators, such as the ones shown in Fig. 1(d), are created by acting simultaneously on all the relevant qudits with highly entangling operations [27,28].

Minimal encoding of non-Abelian anyons.—To simplify the physical requirements for the simulation of G anyons we identify the smallest possible ribbon that can encode the anyonic properties. It is possible to define a ribbon ρ_0, where the direct and dual triangles have support on the *same* qudit, as shown in Fig. 1(e). We define the corresponding ribbon operator as $F^G_{\rho_0} \equiv F^{c,e}_{\rho_0} + \omega F^{c,c}_{\rho_0} + \bar{\omega} F^{c,c^2}_{\rho_0} + \text{H.c.}$, where Hermiticity is explicitly imposed. Explicitly, we have

$$F^G_{\rho_0} = |c\rangle\langle e| + \omega |c^2\rangle\langle c| + \bar{\omega}|e\rangle\langle c^2| + \text{H.c.}, \quad (4)$$

which acts only on three states.

With the minimal string and ribbon operators F^A, F^B, and F^G we can explicitly verify the fusion properties of the $\{A, B, G\}$ subgroup of $D(S_3)$ by acting on a single qudit with six levels. By direct multiplication of the operators given in (2) and (4) we can verify their nontrivial fusion rules. In particular, when two ribbon operators, $F^G_{\rho_0}$, act on top of each other then the G anyons at their endpoints are fused resulting to the ribbon operator of their fusion outcomes, i.e.,

$$F^G_{\rho_0} F^G_{\rho_0} = F^A_{\rho_0} + F^B_{\rho_0} + F^G_{\rho_0}. \quad (5)$$

This fusion process can be realized with a three level system as only the states $|e\rangle$, $|c\rangle$, and $|c^2\rangle$ are involved.

We next consider the braiding properties of G anyons. In the case of the toric code the anyonic statistics of e and m anyons is given in terms of the commutation relations between their ribbon operators $F^e_{\rho_1} F^m_{\rho_2} = R^{em} F^m_{\rho_2} F^e_{\rho_1}$, where ρ_1 and ρ_2 are two crossing paths of e and m anyons, respectively [11]. Because of topological invariance with respect to the exact shape of the path, the braiding relation can be realized by isolating the site, ρ_0, where paths ρ_1 and ρ_2 cross each other. As a result we can take the full system to be site ρ_0, with the anyons positioned outside the system's boundary. Then we have $F^e_{\rho_1 \to \rho_0} = Z_{\rho_0}$ and $F^m_{\rho_2 \to \rho_0} = X_{\rho_0}$ acting on the same qubit at ρ_0, thus obtaining the exchange statistics $R^{em} = -1$ [24,25].

For the $D(S_3)$ model the exchange of two G ribbon operators takes the form [11]

$$F^G_{\rho_1} F^G_{\rho_2} = R^{GG} F^G_{\rho_2} F^G_{\rho_1}, \quad (6)$$

where R^{GG} is given by (1). Hence, to determine R^{GG} we need to implement $F^G_{\rho_1} F^G_{\rho_2}$ and $F^G_{\rho_2} F^G_{\rho_1}$ and compare them. Similarly to the toric code case we employ a single site, ρ_0, and the minimal ribbon operator, $F^G_{\rho_0}$, given in (4), acting on it. As the operators we want to exchange are identical when acting on the single site system we adopt the following prescription. We first identify $F^G_{\rho_1} F^G_{\rho_2}$ with the product of two $F^G_{\rho_0}$ operators as given in (5). Next, to determine $F^G_{\rho_2} F^G_{\rho_1}$, we employ the exchange of their building blocks $F^{h,g}_\rho$,

$$F^{h,g}_{\rho_2} F^{k,l}_{\rho_1} = F^{k,l\bar{g}\bar{h}g}_{\rho_1} F^{h,g}_{\rho_2}, \quad (7)$$

valid for ribbons ρ_1 and ρ_2 with one common end. We employ these relations to compute $F^G_{\rho_2} F^G_{\rho_1}$ and then identify $\rho_1 \to \rho_0$ and $\rho_2 \to \rho_0$ to obtain (see Supplemental Material [33])

$$F^G_{\rho_2} F^G_{\rho_1} = \bar{\omega}(F^A_{\rho_0} + F^B_{\rho_0}) + \omega F^G_{\rho_0}. \quad (8)$$

Direct comparison of (5) and (8) deduces the desired braiding matrix $R^{GG} = \text{diag}(\bar{\omega}, \bar{\omega}, \omega)$ in the $\{A, B, G\}$ basis.

Having a minimal system facilitates the simulation of braiding statistics with current technology. A natural first candidate is to employ current programmable quantum computers, such as the commercial qubit-based IBM device, to implement the ribbon operator $F^G_{\rho_0}$. As $F^G_{\rho_0}$ is nonunitary it cannot be straightforwardly implemented with unitary quantum logic gates [34]. However, as for any matrix, a unitary block encoding [35–39] can be constructed where $F^G_{\rho_0}$ is embedded within a larger unitary, U_F. Through the preparation and measurement of a subset of qubits, a quantum circuit describing U_F allows for $F^G_{\rho_0}$ to be applied to the labeled qutrit state. Based on the singular value decomposition of $F^G_{\rho_0}$ [40], U_F must act on a minimum of three qubits (see Supplemental Material [33]). Up to a rescaling of $F^G_{\rho_0}$, the success probability p of implementing the transformation on pure states is bounded as $1/4 \le p \le 1$. Compiling an explicit U_F using the native qiskit transpiler into the typical device gate set (e.g., single qubit rotations + CNOT) gives a circuit depth

of 74 operations with 20 CNOTs [41]. Using a simplified model of current device noise, we simulated the circuits applying this U_F to states that maximize and minimize the success probability of applying $F^G_{\rho_0}$ to the labeled qutrit state (see Supplemental Material [33]). We observe low fidelities between the idealized circuits and the noisy implementations, indicating that the qubit encoding suffers large overheads for these operations. We note that this is a fully programmable, circuit-based system. One expects that directly engaging the hardware could lead to better results. For example, developing block encodings based on entangling qubit-qutrit unitaries could fair better. However at present commercially available circuit-level transpilers are unavailable for such entangling gates. To implement such gates would require moving toward bespoke functionality such as pulse-level control, which is an active area of research [42–45]. As an alternative, we resort to a photonic platform that can both encode qutrits and perform nonunitary operations in a straightforward way.

Experimental photonic simulation.—Here, we show how a classical photonic simulator can accurately perform the nonunitary operations needed to realize the fusion and braiding properties of the G non-Abelian $D(S_3)$ anyons with minimal errors. We experimentally implement the ribbon operator $F^G_{\rho_0}$, that encodes two G anyons at its endpoints, and its compositions $F^G_{\rho_1}F^G_{\rho_2}$ and $F^G_{\rho_2}F^G_{\rho_1}$ given in (4), (5), and (8), respectively. The experiment consists of three distinct parts, as shown in Fig. 2(a). First, we generate a qutrit state encoded in the transverse-spatial degree of freedom of light. We then evolve the state through the desired operations programmed on our photonic simulator. Finally, we characterize the implemented operations via quantum process tomography.

The qutrit is encoded in a transverse-spatial modal basis consisting of discrete macro-pixels, as shown in Fig. 2(b). We choose this particular basis as it can be tailored to perform high-quality projective measurements [47,48]. Next, the qutrit state is evolved through the G ribbon operator (4) and its compositions (5) and (8), following which it is mapped onto spatially separated outcomes that can be measured on a camera. These operations are by definition nonunitary. Therefore, the task of performing an operation and sorting the outcomes spatially can be mapped to the problem of state discrimination between nonorthogonal states. There exist multiple schemes that perform this task by compromising either efficiency or accuracy of the discrimination [49]. As we are interested in simulating the anyonic properties, we choose to enhance the accuracy of the operations at the expense of efficiency through optical losses. Herein we use the formalism of unambiguous state discrimination [50–53], where one employs auxiliary modes to embed a low-dimensional nonunitary operation within a higher-dimensional unitary. The outcomes corresponding to the auxiliary modes can be ignored since they provide no information about the input state, and thus correspond to loss.

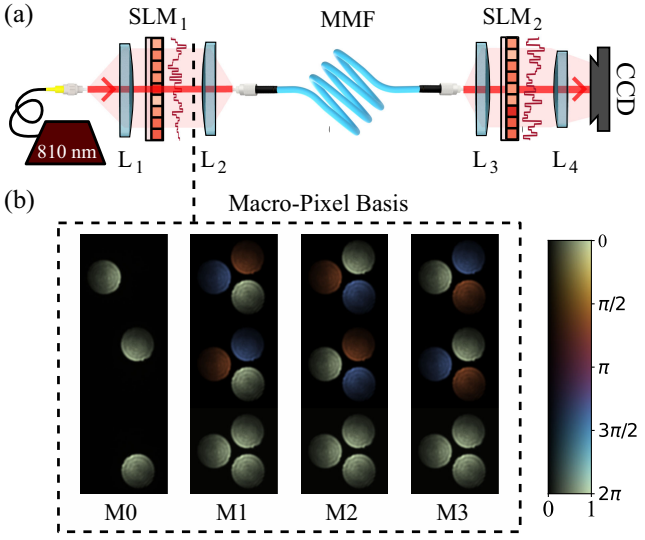

FIG. 2. (a) Experimental Setup. A coherent light source (810 nm) is incident on a phase-only spatial light modulator (SLM_1) and then coupled into a 2 m-long graded-index multimode fiber (MMF) with core diameter 50 μm. The output of the MMF is incident on SLM_2 followed by a CCD camera. The combination of a high-dimensional mode mixer (MMF) sandwiched between two phase planes (SLM_1 and SLM_2) serves as a programmable optical circuit that can encode any nonunitary operations as shown in [46]. Additionally, SLM_2 is used for performing projective measurements required for quantum process tomography (QPT) to check the fidelity of the implemented transformations $\mathbf{T} \in \{F^G_{\rho_0}, F^G_{\rho_1}F^G_{\rho_2}, F^G_{\rho_2}F^G_{\rho_1}\}$. (b) Qutrit encoding. Images showing three-dimensional photonic transverse-spatial modes in the macro-pixel basis (M0) generated by SLM_1. Modes from all mutually unbiased bases (M1, M2, M3) of the three-dimensional macro-pixel basis are also shown, which are used for performing QPT.

Interestingly, the three operations we aim to implement, $\mathbf{T} \in \{F^G_{\rho_0}, F^G_{\rho_1}F^G_{\rho_2}, F^G_{\rho_2}F^G_{\rho_1}\}$, are Hermitian and have symmetric overlaps between different columns, i.e., $|T_{rj} \cdot T^*_{ri\neq j}| = \alpha$, $\forall\ r$ where T_{rc} corresponds to the rth row and cth column of the given $\mathbf{T}$ matrix. This allows us to use a single auxiliary mode to perform these operations [54] as was recently shown to be experimentally viable with optical circuits [55]. Because of the nonunitarity, these operations cannot be performed with unit success probability. Theoretically, the maximum average success probabilities are 50%, 37.5%, and 75% for $F^G_{\rho_0}$, $F^G_{\rho_1}F^G_{\rho_2}$, and $F^G_{\rho_2}F^G_{\rho_1}$, respectively. Using this approach, we encode our three-dimensional Hermitian operators into four-dimensional unitaries to proceed with this task.

These unitary operations are implemented using the recently demonstrated "top-down" approach, where an arbitrary optical circuit is embedded within a higher-dimensional mode mixer sandwiched between two programmable phase planes [46]. Our circuit uses a commercial multimode fiber (MMF) as a mode mixer that is placed between two programmable spatial light modulators (SLMs)

TABLE I. Experimental results for the best case fidelity and purity of the processes corresponding to the $F^G_{\rho_0}$, $F^G_{\rho_1}F^G_{\rho_2}$, and $F^G_{\rho_2}F^G_{\rho_1}$ operations. The error values are reported up to 3 standard deviations and correspond to systematic misalignment error (see Supplemental Material [33]).

Operation (**T**)	Fidelity $(\mathcal{F}(\rho_{\mathcal{T}}, \rho_{\tilde{\mathcal{T}}}))$	Purity $\mathcal{P}((\rho_{\tilde{\mathcal{T}}}))$
$F^G_{\rho_0}$	$95.23 \pm 0.93\%$	$96.04 \pm 0.03\%$
$F^G_{\rho_1}F^G_{\rho_2}$	$94.44 \pm 0.85\%$	$97.65 \pm 0.05\%$
$F^G_{\rho_2}F^G_{\rho_1}$	$97.59 \pm 0.59\%$	$94.43 \pm 0.06\%$

as shown in Fig. 2(a). We use an inverse design technique known as the wavefront-matching (WFM) algorithm to program the SLMs. The WFM algorithm calculates the phase plane solutions by iteratively maximizing the overlap between a set of input fields with the desired output ones. After updating the SLMs with the phase solutions given by the WFM algorithm, we couple a coherent light source with a wavelength of 810 nm to characterize the implemented operation. The statistics of a single-photon qutrit state propagating through the system are identical to those obtained for a coherent state, allowing us to simplify the experiment and use a camera for detection [56].

We perform quantum process tomography to quantify the fidelity of the implemented operations $\tilde{\mathbf{T}}$ in relation to the ideal operations **T**. Note that in addition to both SLMs being used for implementing the target operation **T**, SLM_1 is used for generating the complete set of input modes [macro-pixel mutually unbiased bases M0–M3, Fig. 2(b)] and SLM_2 is used for performing the projective measurements needed for quantum process tomography (QPT). For each input mode, we measure the intensity at each of the three designated output modes at the camera, ignoring the auxiliary output. Next, SLM_2 is used to sequentially project the output into all mutually unbiased bases of the desired output modes. This is done in a manner similar to how projective measurements are performed with an SLM and a single mode fiber [57], with the center region of the CCD camera used in place of the single mode fiber. Using these measurements, we construct a coupling matrix between the complete set of input and output modes. This coupling matrix is then used to recover the implemented process via QPT, which we represent via its Choi state, $\rho_{\tilde{\mathcal{T}}} = \tilde{\mathcal{T}} \otimes \mathbb{1}(\rho^+)$, where ρ^+ is the maximally entangled state. The Choi state captures complete information about the process and can be used to evaluate the purity and fidelity to the target operations (see Supplemental Material [33]) [46].

We implement ten realizations of each operation $F^G_{\rho_0}$, $F^G_{\rho_1}F^G_{\rho_2}$, and $F^G_{\rho_2}F^G_{\rho_1}$, and reconstruct their processes using the methods described above. Since different positions of measurement outcomes result in different performance, we vary the positions of measurement outcomes on the camera in each realization in order to realize the best possible

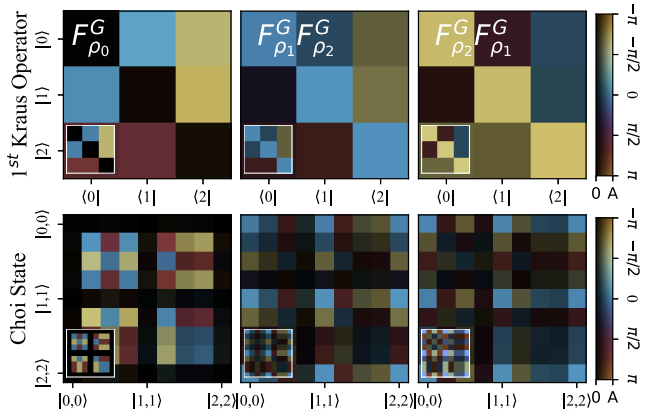

FIG. 3. Experimentally measured operators. We obtain the leading Kraus operator from the tomographed process (top row) and the Choi state representation for each operator $F^G_{\rho_0}$, $F^G_{\rho_1}F^G_{\rho_2}$, and $F^G_{\rho_2}F^G_{\rho_1}$ (bottom row) (see Supplemental Material [33]). Insets show theoretically expected results in each plot. $|A|$ corresponds to the maximum amplitude for a given plot and respective inset.

implementation of these operators. Out of all the implementations, the best case fidelities, $\mathcal{F}$, and purities, $\mathcal{P}$, of the process for each operation $F^G_{\rho_0}$, $F^G_{\rho_1}F^G_{\rho_2}$, and $F^G_{\rho_2}F^G_{\rho_1}$ are shown in Table I. To visualize the quality of these operations, it is convenient to use the Kraus representation, which is an alternative way to represent these processes (see Supplemental Material [33]). The ideal target operations have only one nonzero Kraus operator, which we can compare to the leading Kraus operators of the implemented processes owing to their high purity. Figure 3 (top row) depicts the leading Kraus operator of the implemented processes, showing that it agrees well with the target operations (insets). The full Choi state representation of these high purity processes is shown in Fig. 3 (bottom row), with the ideal state shown for comparison.

Conclusions.—Non-Abelian anyons present a fascinating and promising avenue for fault-tolerant quantum computation. Emulating their complex braiding statistics has so far evaded experimental realization. In this Letter, we have demonstrated a photonic simulation of the ribbon operators corresponding to $D(S_3)$ non-Abelian anyons with fidelities and purities above 94%. Our simulation has certified the minimal requirements and operations necessary to identify the statistics of these anyons. This represents a significant step forward in the experimental study of non-Abelian anyons and opens the door to future efforts toward experimentally realizing more complex manipulations and applications of these exotic systems. Extending our experimental scheme to small-scale multiqudit quantum systems [58–60] can potentially unlock the applications of non-Abelian anyons and the demonstration of their fault tolerance against local perturbations. For example, two qutrits encoded in a nine-dimensional photonic system

or in a scalable architecture with Josephson junctions or ion traps [61] could be employed to encode distinguishable F_ρ^G ribbon operators where both the F_{GGG}^G and R^{GG} matrices can be realized. Nevertheless, extending it to a fully scalable system still remains a formidable challenge.

We are grateful to Gavin Brennen, Sofyan Iblisdir, and James Wootton for helpful discussions. This work was made possible by financial support from the QuantERA ERA-NET Co-fund (FWF Project No. I3773-N36), the UK Engineering and Physical Sciences Research Council (EPSRC) (EP/P024114/1, EP/R020612/1, and EP/W003252/1), European Research Council (ERC) Starting Grant No. PIQUaNT (No. 950402).

*These authors contributed equally to this work.
†Corresponding author: m.malik@hw.ac.uk
‡Corresponding author: j.k.pachos@leeds.ac.uk

[1] J. M. Leinaas and J. Myrheim, On the theory of identical particles, Il Nuovo Cimento B (1971–1996) **37**, 1 (1977).
[2] Frank Wilczek, Quantum mechanics of fractional-spin particles, Phys. Rev. Lett. **49**, 957 (1982).
[3] F. Alexander Bais, Peter van Driel, and Mark de Wild Propitius, Quantum symmetries in discrete gauge theories, Phys. Lett. B **280**, 63 (1992).
[4] Hoi-Kwong Lo and John Preskill, Non-Abelian vortices and non-Abelian statistics, Phys. Rev. D **48**, 4821 (1993).
[5] Vatshal Srivastav, Utso Bhattacharya, and Amit Dutta, Dynamical quantum phase transitions in extended toric-code models, Phys. Rev. B **100**, 144203 (2019).
[6] Dong-Ling Deng, Xiaopeng Li, and S. Das Sarma, Machine learning topological states, Phys. Rev. B **96**, 195145 (2017).
[7] Gavin K. Brennen and Jiannis K. Pachos, Why should anyone care about computing with anyons, Proc. R. Soc. A **464**, 1 (2008).
[8] A. Yu. Kitaev, Unpaired Majorana fermions in quantum wires, Phys. Usp. **44**, 131 (2001).
[9] R. Raussendorf, J. Harrington, and K. Goyal, Topological fault-tolerance in cluster state quantum computation, New J. Phys. **9**, 199 (2007).
[10] Chetan Nayak, Steven H. Simon, Ady Stern, Michael Freedman, and Sankar Das Sarma, Non-Abelian anyons and topological quantum computation, Rev. Mod. Phys. **80**, 1083 (2008).
[11] A. Yu Kitaev, Fault-tolerant quantum computation by anyons, Ann. Phys. (Amsterdam) **303**, 2 (2003).
[12] Jiannis K. Pachos, *Introduction to Topological Quantum Computation* (Cambridge University Press, Cambridge, England, 2012).
[13] Sankar Das Sarma, Michael Freedman, and Chetan Nayak, Topologically protected qubits from a possible non-Abelian fractional quantum Hall state, Phys. Rev. Lett. **94**, 166802 (2005).
[14] N. Read and Dmitry Green, Paired states of fermions in two dimensions with breaking of parity and time-reversal symmetries and the fractional quantum Hall effect, Phys. Rev. B **61**, 10267 (2000).
[15] D. A. Ivanov, Non-Abelian statistics of half-quantum vortices in p-wave superconductors, Phys. Rev. Lett. **86**, 268 (2001).
[16] P. Yu, J. Chen, M. Gomanko, G. Badawy, E. P. A. M. Bakkers, K. Zuo, V. Mourik, and S. M. Frolov, Non-Majorana states yield nearly quantized conductance in proximatized nanowires, Nat. Phys. **17**, 482 (2021).
[17] James R. Wootton, Demonstrating non-Abelian braiding of surface code defects in a five qubit experiment, Quantum Sci. Technol. **2**, 015006 (2017).
[18] Jin-Shi Xu, Kai Sun, Yong-Jian Han, Chuan-Feng Li, Jiannis K. Pachos, and Guang-Can Guo, Simulating the exchange of Majorana zero modes with a photonic system, Nat. Commun. **7**, 13194 (2016).
[19] Jin-Shi Xu, Kai Sun, Jiannis K. Pachos, Yong-Jian Han, Chuan-Feng Li, and Guang-Can Guo, Photonic implementation of Majorana-based berry phases, Sci. Adv. **4**, eaat6533 (2018).
[20] Zheng-Hao Liu, Kai Sun, Jiannis K. Pachos, Mu Yang, Yu Meng, Yu-Wei Liao, Qiang Li, Jun-Feng Wang, Ze-Yu Luo, Yi-Fei He, Dong-Yu Huang, Guang-Rui Ding, Jin-Shi Xu, Yong-Jian Han, Chuan-Feng Li, and Guang-Can Guo, Topological contextuality and anyonic statistics of photonic-encoded parafermions, PRX Quantum **2**, 030323 (2021).
[21] T. I. Andersen *et al.*, Observation of non-abelian exchange statistics on a superconducting processor, arXiv:2210.10255.
[22] John P. T. Stenger, Nicholas T. Bronn, Daniel J. Egger, and David Pekker, Simulating the dynamics of braiding of Majorana zero modes using an IBM quantum computer, Phys. Rev. Res. **3**, 033171 (2021).
[23] Rajeev Acharya *et al.*, Suppressing quantum errors by scaling a surface code logical qubit, Nature (London) **614**, 676 (2023).
[24] Chao-Yang Lu, Wei-Bo Gao, Otfried Guhne, Xiao-Qi Zhou, Zeng-Bing Chen, and Jian-Wei Pan, Demonstrating anyonic fractional statistics with a six-qubit quantum simulator, Phys. Rev. Lett. **102**, 030502 (2009).
[25] J. K. Pachos, W. Wieczorek, C. Schmid, N. Kiesel, R. Pohlner, and H. Weinfurter, Revealing anyonic features in a toric code quantum simulation, New J. Phys. **11**, 083010 (2009).
[26] Xi-Wang Luo, Yong-Jian Han, Guang-Can Guo, Xingxiang Zhou, and Zheng-Wei Zhou, Simulation of non-Abelian anyons using ribbon operators connected to a common base site, Phys. Rev. A **84**, 052314 (2011).
[27] M. Aguado, G. K. Brennen, F. Verstraete, and J. I. Cirac, Creation, manipulation, and detection of abelian and non-Abelian anyons in optical lattices, Phys. Rev. Lett. **101**, 260501 (2008).
[28] G K Brennen, M Aguado, and J I Cirac, Simulations of quantum double models, New J. Phys. **11**, 053009 (2009).
[29] Salman Beigi, Peter W. Shor, and Daniel Whalen, The quantum double model with boundary condensations and symmetries, Commun. Math. Phys. **306**, 663 (2011).
[30] Anna Kómár and Olivier Landon-Cardinal, Anyons are not energy eigenspaces of quantum double Hamiltonians, Phys. Rev. B **96**, 195150 (2017).
[31] Katharina Laubscher, Daniel Loss, and James R. Wootton, Universal quantum computation in the surface code using non-Abelian islands, Phys. Rev. A **100**, 012338 (2019).

[32] James R. Wootton, Jan Burri, Sofyan Iblisdir, and Daniel Loss, Error correction for non-Abelian topological quantum computation, Phys. Rev. X **4**, 011051 (2014).
[33] See Supplemental Material at http://link.aps.org/supplemental/10.1103/PhysRevLett.132.110601 for the theoretical derivations and for the details of the experiment.
[34] Michael A Nielsen and Isaac Chuang, *Quantum Computation and Quantum Information* (American Association of Physics Teachers, Cambridge, 2002).
[35] Daan Camps, Lin Lin, Roel Van Beeumen, and Chao Yang, Explicit quantum circuits for block encodings of certain sparse matrice, arXiv:2203.10236.
[36] András Gilyén, Yuan Su, Guang Hao Low, and Nathan Wiebe, Quantum singular value transformation and beyond exponential improvements for quantum matrix arithmetics, in *Proceedings of the 51st Annual ACM SIGACT Symposium on Theory of Computing* (2019), pp. 193–204; arXiv:1806.01838.
[37] Guang Hao Low and Isaac L. Chuang, Optimal Hamiltonian simulation by quantum signal processing, Phys. Rev. Lett. **118**, 010501 (2017).
[38] Guang Hao Low and Isaac L. Chuang, Hamiltonian simulation by qubitization, Quantum **3**, 163 (2019).
[39] D. Camps and R. Van Beeumen, Fable: Fast approximate quantum circuits for block-encodings, in *Proceedings of the 2022 IEEE International Conference on Quantum Computing and Engineering (QCE)* (IEEE Computer Society, Los Alamitos, CA, USA, 2022), pp. 104–113; arXiv:2205.00081.
[40] Roger A. Horn and Charles R. Johnson, *Matrix Analysis*, 2nd ed. (Cambridge University Press, Cambridge, England, 2012).
[41] Qiskit an open-source framework for quantum computing (2022), https://www.ibm.com/quantum/qiskit.
[42] Noah Goss, Alexis Morvan, Brian Marinelli, Bradley K. Mitchell, Long B. Nguyen, Ravi K. Naik, Larry Chen, Christian Jünger, John Mark Kreikebaum, David I. Santiago *et al.*, High-fidelity qutrit entangling gates for superconducting circuits, Nat. Commun. **13**, 7481 (2022).
[43] Ha C. Nguyen, Bao G. Bach, Tien D. Nguyen, Duc M. Tran, Duy V. Nguyen, and Hung Q. Nguyen, Simulating neutrino oscillations on a superconducting qutrit, Phys. Rev. D **108**, 023013 (2023).
[44] Alexey Galda, Michael Cubeddu, Naoki Kanazawa, Prineha Narang, and Nathan Earnest-Noble, Implementing a ternary decomposition of the toffoli gate on fixed-frequencytransmon qutrits, arXiv:2109.00558.
[45] Machiel S. Blok, Vinay V. Ramasesh, Thomas Schuster, Kevin O'Brien, John-Mark Kreikebaum, Dar Dahlen, Alexis Morvan, Beni Yoshida, Norman Y. Yao, and Irfan Siddiqi, Quantum information scrambling on a superconducting qutrit processor, Phys. Rev. X **11**, 021010 (2021).
[46] Suraj Goel, Saroch Leedumrongwatthanakun, Natalia Herrera Valencia, Will McCutcheon, Claudio Conti, Pepijn W. H. Pinkse, and Mehul Malik, Inverse-design of high-dimensional quantum optical circuits in a complex medium, arXiv:2204.00578.
[47] Natalia Herrera Valencia, Vatshal Srivastav, Matej Pivoluska, Marcus Huber, Nicolai Friis, Will McCutcheon, and Mehul Malik, High-dimensional pixel entanglement efficient generation and certification, Quantum **4**, 376 (2020).
[48] Vatshal Srivastav, Natalia Herrera Valencia, Saroch Leedumrongwatthanakun, Will McCutcheon, and Mehul Malik, Characterizing and tailoring spatial correlations in multimode parametric down-conversion, Phys. Rev. Appl. **18**, 054006 (2022).
[49] Stephen M. Barnett and Sarah Croke, Quantum state discrimination, Adv. Opt. Photonics **1**, 238 (2009), 0810.1970.
[50] I. D. Ivanovic, How to differentiate between non-orthogonal states, Phys. Lett. A **123**, 257 (1987).
[51] Anthony Chefles, Unambiguous discrimination between linearly independent quantum states, Phys. Lett. A **239**, 339 (1998).
[52] Anthony Chefles and Stephen M. Barnett, Strategies for discriminating between non-orthogonal quantum states, J. Mod. Opt. **45**, 1295 (1998).
[53] S. Franke-Arnold and J. Jeffers, Unambiguous state discrimination in high dimensions, Eur. Phys. J. D **66**, 196 (2012).
[54] Megan Agnew, Eliot Bolduc, Kevin J. Resch, Sonja Franke-Arnold, and Jonathan Leach, Discriminating single-photon states unambiguously in high dimensions, Phys. Rev. Lett. **113**, 020501 (2014), 1403.3830.
[55] Suraj Goel, Max Tyler, Feng Zhu, Saroch Leedumrongwatthanakun, Mehul Malik, and Jonathan Leach, Simultaneously sorting overlapping quantum states of light, Phys. Rev. Lett. **130**, 143602 (2023).
[56] Stephen M. Barnett, On single-photon and classical interference, Phys. Scr. **97**, 114004 (2022).
[57] Frédéric Bouchard, Natalia Herrera Valencia, Florian Brandt, Robert Fickler, Marcus Huber, and Mehul Malik, Measuring azimuthal and radial modes of photons, Opt. Express **26**, 31925 (2018).
[58] Manuel Erhard, Mehul Malik, Mario Krenn, and Anton Zeilinger, Experimental Greenberger–Horne–Zeilinger entanglement beyond qubits, Nat. Photonics **12**, 759 (2018).
[59] Stefano Paesani, Jacob F. F. Bulmer, Alex E. Jones, Raffaele Santagati, and Anthony Laing, Scheme for universal high-dimensional quantum computation with linear optics, Phys. Rev. Lett. **126**, 230504 (2021).
[60] Alba Cervera-Lierta, Mario Krenn, Al'an Aspuru-Guzik, and Alexey Galda, Experimental high-dimensional Greenberger-Horne-Zeilinger entanglement with superconducting transmon qutrits, Phys. Rev. Appl. **17**, 024062 (2022).
[61] Martin Ringbauer, Michael Meth, Lukas Postler, Roman Stricker, Rainer Blatt, Philipp Schindler, and Thomas Monz, A universal qudit quantum processor with trapped ions, Nat. Phys. **18**, 1053 (2022).